EXPERIMENTAL OBSERVATIONS TO THE ELECTRICAL FIELD FOR ELECTROREFINING OF SPENT NUCLEAR FUEL IN THE MARK-IV ELECTROREFINER

by

S. X. Li, T. Sofu, and R. A. Wigeland

Technology Development Division
Argonne National Laboratory-West
P. O. Box 2528
Idaho Falls, ID 83403-2528

To be Presented
at
193rd Meeting of the Electrochemical Society
XI--Eleventh International Symposium on Molten Salts

May 1998

*Work supported by the U.S. Department of Energy, Reactor Systems, Development and Technology, under Contract W-31-109-Eng-38.

DISCLAIMER

EXPERIMENTAL OBSERVATIONS IN RELATION TO THE ELECTRICAL FIELD FOR ELECTROREFINING OF SPENT NUCLEAR FUEL IN THE MARK-IV ELECTROREFINER

S. X. Li, T. Sofu, and R. A. Wigeland
Argonne National Laboratory
Idaho Falls, ID 83403

ABSTRACT

Experimental results from the pilot scale electrorefiner (Mark-IV ER) treating spent nuclear fuel are reported in this article. The electrorefining processes were carried out in a LiCl-KCl-UCl_3 electrolyte. It has been noted that a pool of molten cadmium below the electrolyte plays an important role in the electrorefining operations. In addition, formations of electrical shorting path between anode baskets and the electrorefiner vessel were observed, which lessened the uranium dissolution process from anode baskets, however appeared to improve the morphology of cathode deposit. The FIDAP simulation code was used to calculate the electrical potential field distributions and the potential gradient near the cathode. The effect of the electrical shorting between anode baskets and electrorefiner vessel on the morphology of cathode products is discussed.

1. INTRODUCTION

Argonne National Laboratory (ANL) is currently demonstrating an electrometallurgical process for treatment of spent nuclear fuel from the Experimental Breeder Reactor-II (EBR-II) (1). One of the key steps in the spent fuel treatment process is electrorefining. The electrorefiner (Mark-IV ER) is located in the Fuel Conditioning Facility (FCF) at the ANL-West site in Idaho.

Figure 1 shows the major internal and external components of the Mark-IV ER. The ER vessel is made of stainless steel with the inside diameter of 100 cm. The vessel contains a bottom layer of ~ 10 cm molten cadmium and a 32 cm top layer of molten LiCl-KCl eutectic containing ~ 10 wt% of UCl_3. The ER operating temperature is held at 450°C or 500°C. Figure 2 shows the relative positions of the four ports in the ER, labeled A, B, C, and D. During an electrorefining process, PortB and/or PortD can be configured as the anodes and PortA and/or PortC can be configured as the cathodes. The cadmium pool can also be used as an electrode for electrorefining. Its polarity depends on its use as either anode or cathode. There are two Ag/AgCl reference electrodes installed in the ER

as shown in Figure 2. The voltage differences between the reference electrodes and the ER vessel or each port can be measured during electrorefining processes.

The characteristics of the electrorefining processes at the Mark-IV ER include pilot scale, large batch size, irradiated fuel, high temperature, and remote operations.

The spent driver fuel consists of uranium, zirconium, bond sodium, and fission products. The primary purpose of the electrorefining is to separate uranium from other fuel components. For this purpose, the fuel elements with cladding are chopped into segments of ~ 0.635 cm in length and placed in fuel dissolution baskets (FDBs). The FDBs are made of stainless steel. During an electrorefining, the FDBs filled with fuel segments can be the anode and a steel mandrel can be the cathode. First in the process, the bond sodium and active metal fission products will chemically react and displace UCl_3 from the molten salt. Uranium will then be electrochemically dissolved from the fuel segments and deposit onto the cathode. Zirconium and noble metal fission products are ideally retained in the cladding hulls.

There are two types of outputs after electrorefining the spent nuclear fuel, cladding hulls, with most of zirconium and noble metal fission products retained, and cathode products made of uranium metal. This article summarizes experimental results obtained during the electrorefining of the spent nuclear fuel in the Mark-IV ER. The analyses focus on the cathodic processes, which include uranium recovery efficiency, current efficiency, pulsating current effects, and the impact of electrical potential field distributions on morphology of the cathode products. The electrical potential field distributions calculated by numerical simulations are used in interpreting the experimental results. The experience with anodic processes is published in a separate article (2).

2. EXPERIMENTAL OBSERVATIONS AND RESULTS

2.1. The Cadmium Pool in Mark-IV ER

2.1.1 The Cadmium Pool as Uranium Collector. Two kinds of transport modes can be configured in the Mark-IV ER to deposit uranium onto a cathode mandrel. One is called direct transport, during which the anode is chopped fuel segments in fuel dissolution baskets and the cathode is a steel mandrel. Another is called deposition, during which the anode is the cadmium pool with dissolved uranium and the cathode is a steel mandrel.

Considerable experience gained during electrolytic deposition of metals from molten salt shows that cathodic deposits have a basically dendritic or powdery structure. The dendritic deposits have been observed by several investigators during the electrorefining of uranium (3,4). Therefore, one of the major purpose to keep a cadmium layer in the Mark-IV ER is to collect the uranium dendrites dropped during electrorefinings. Uranium debris may result from side or bottom scrapers shaping the excess materials off

as the deposit grows or the loose dendritic deposit falling off by itself. The dropped uranium will dissolve in the cadmium pool and can be recovered by a deposition process.

2.1.2. The Cadmium Pool as an Intermediate Electrode during Direct Transport Processes. When performing direct transport operations in the Mark-IV ER, a *dc* current is applied between an anode (FDBs) and a cathode (steel mandrel). Since both anode and cathode are in the salt phase, it looks as if the current distribution would be only in the salt phase during a direct transport and the cadmium pool would not be involved. However, it has been noticed that the voltage readings between reference electrodes and the ER vessel changed dramatically during direct transport operations. Figure 3 gives an example of how the voltage readings between the reference electrodes and ER vessel vary as the applied current varies during a direct transport process.

The voltage readings measured between the reference electrodes and the ER vessel represent voltage changes at the salt/cadmium interface. Variations in these voltages indicate that there must be electrochemical reactions taking place at the salt/cadmium interface during the direct transport process. In order to interpret the reference electrode readings shown in Figure 3, a conceptual model was developed for a direct transport process in the ER. A schematic of the model is given in Figure 4.

According to the model shown in Figure 4, a portion of applied external current will pass through the cadmium pool during a direct transport process because the resistivity of the molten salt at 500°C is 1.8×10^8 times the resistivity of liquid cadmium (5,6). The current passing through the cadmium pool results in reduction reactions at the salt/cadmium interface close to the anode baskets and oxidation reactions at salt/cadmium interface close to the cathode mandrel. The cadmium pool performs as an intermediate electrode during direct transport processes in the Mark-IV ER. The redox reaction, $U^{3+} \rightleftarrows U(Cd)$, is used as an example in Figure 4. Other redox reactions can take place at the interface as well depending on chemical compositions at the interface and magnitude the of external current applied.

The plot of reference electrode voltage readings during the Cathode No. 29 run (Figure 3) gives a good example to verify the proposed model. For reference electrode A, which was close to the anode, Figure 3 shows the voltage readings decreased once the direct transport process was started. This is an indication that U^{3+} was reduced to uranium metal and dissolved into cadmium at the salt/cadmium interface close to the anode basket. The voltage readings of reference electrode B, which was close to the cathode, gradually increased from the start of the direct transport process. The voltage reached an apex value of -0.95 V after ~14 hours, and then gradually decreased. The variations in voltage readings of the reference electrode B can also be explained by the proposed model. At the start of the direct transport process, the surface area at the anode was much larger than that at the cathode. Therefore, the current density passing through salt/cadmium interface close to the cathode (Figure 4) was much higher than that passing through the interface close to the

anode. The uranium in cadmium solution close to the cathode was depleting, which caused the voltage reading of reference electrode B to increase. As the direct transport process continued, the cathode surface area gradually increased and the current density passing through the interface close to the cathode gradually decreased. The rate of uranium depleting from the cadmium pool decreased. This combined effect results in the reference electrode voltage reaching its apex at ~ 14 hours as previously mentioned.

The electrical potential field calculations for direct transports in the Mark-IV ER have been carried out by using FIDAP simulation code. The simulation results confirm that the cadmium pool acts as an intermediate electrode during a direct transport. The potential of the cadmium pool is lower than that of the anode but higher than that of the cathode (7). A comparable result has also been reported by T. Kobayashi et al. (8). By numerically simulating the electrochemical processes in a new ER, which has a nonconductive ceramic partition between the anode and cathode salt regions, they concluded that since the two salt regions are electrically connected via a Cd pool at the bottom, the Cd pool acts as an intermediate electrode between the anode and the cathode.

2.1.3. Decreasing in Cadmium Level. The Mark-IV ER was loaded with 431 kg of cadmium in December 1994. The measured cadmium level after the loading was 9.86 cm. It has been observed since then that the cadmium level has gradually decreased. Figure 5 shows the measured cadmium level from January 1995 to November 1997. Simulated cadmium level data are also given in the figure for comparison. The simulation was carried out using thermodynamic equilibriums. It can be seen in Figure 5 that although the measured values fluctuate, they are significantly lower than the predicted values by simulation.

It is believed that the decrease in cadmium level is mainly due to the high vapor pressure and high vaporization rate of cadmium at the ER operational temperature of 500°C (9), and to the relatively cool temperatures above the molten salt. Cadmium vapor can migrate through the salt phase and deposit on the metal surfaces in the ER cover gas space. A reduction in the ER operating temperature, from 500°C to 450°C in September 1996, and the installation of a cadmium vapor trap in April 1997 attempted to mitigate the vapor deposition problem. However, as of the measurement in November 1997, the cadmium level in the Mark-IV ER continued to drop (Figure 5).

2.1.4. Low Cadmium level Resulting in Electrical Shorting between Anode Baskets and ER Vessel. The decrease in the cadmium level has caused an unexpected problem for the ER operations, an electrical shorting between anode baskets and ER vessel hardware. Figure 6 shows schematically how the electrical shorting developed. As indicated in Figure 6, there is a metal ring beneath each port in the ER. The two cathode port rings have beryllia bottom scrapers on their tops while two anode port rings have bare metal surfaces. The height of the metal rings is 9.84 cm from inside bottom of the vessel. When the cadmium level is below 9.84 cm, surfaces of the metal rings will be exposed into the salt phase. During a direct transport, the potential of the cadmium pool is lower than that of the anode

baskets. Uranium will deposit on the exposed surface of the ring beneath the anode baskets. The deposit will gradually accumulate and finally reach the FDBs, which forms an electrical shorting path between the anode baskets and the ER vessel.

The electrical shorting between anode baskets and hardware inside the Mark-IV ER vessel has been observed since November 1996 when the cadmium level was at ~9.6 cm. The typical voltage and current traces which indicate the shorting taking place during a direct transport are shown in Figure 7. The evidences of the shorting are the fluctuations in anodic voltage and cell current signals. Presence of the shorting has made uranium dissolution from anode baskets difficult, and direct transport operations prolonged.

In order to solve the electrical shorting problem, 55 kg of cadmium metal was added into the ER in July 1997, which raised cadmium level from 9.22 cm to 10.29 cm and should submerge the metal rings beneath the anode ports. The ER operational temperature was increased from 450°C to 500°C in August 1997, which raised the cadmium level from 10.29 cm to 10.57 cm. Since then, no similar electrical shorting has been observed during direct transport runs. The typical voltage and current traces without the shorting are given in Figure 8.

2.2. Morphology of Cathode Deposit Improved by Electrical Shorting between Anode Baskets and ER Vessel

The experimental results presented above have indicated that the electrical shorting between anode baskets and vessel hardware is detrimental to the uranium dissolution processes during the spent fuel treatments in the Mark-IV ER. However, some beneficial effects of the shorting on the electrorefining have also been observed.

Table I summarizes experimental results from production of irradiated cathodes by direct transports in Mark-IV ER. The third column in the table, "Uranium Recovered by DT Process," is calculated by uranium mass collected on the cathode divided by the total uranium mass in the feed, nominally 8.1 kg uranium in the fuel and 1.4 kg uranium reduced by bond sodium and active metal fission products. The sixth column in the table, "~Shorting A-h," is the estimated ampere-hours of the shorting time period during the run. The "shorting" is defined as when the anode voltage becomes very unstable. Figure 7 shows how the "Shorting" and "Shorting A-h" are estimated. It is interesting to note that the uranium recovered by a direct transport process is proportional to the "Shorting Ampere-hours" occurring during the electrorefining process. The more severe the shorting, the more uranium was recovered. For instance, cathode No. 49 had the worst shorting, existing during almost the entire run, and had the best uranium recovery result. It appears that the electrical shorting between anode baskets and the ER vessel must have benefited the stability of nucleation or electrocrystallization processes on the cathode.

Besides the electrical shorting, the experimental results given in Table I may have been affected by the other ER operational parameters such as cell voltage and mixing

conditions. Table II lists the experimental results of three direct transport runs under different shorting, but otherwise similar, operating conditions. Data given in Table II show clearly that the amount of uranium recovered through the direct transports is improved by existence of the shorting. Photographs of the three cathodes are given in Figure 9 (a), (b), and (c).

Table I. Summary of Irradiated Cathodes Produced by Direct Transport in Mark-IV ER (from June 1996 to November 1997)

Cathode No.	U Mass on Cathode, kg	Uranium Recovered By DT Process[a]	ER Temperature	Total A-h	~Shorting A-h	Current Efficiency
39	5.5	64%	450C	3136	2500	59%
43	6.2	65%	450C	3296	2990	64%
45	7.3	74%	450C	3640	3200	68%
48	8.6	90%	450C	4810	4400	60%
49	9.1	95%	450C	4628	4500	66%
50	4.4	46%	450C	2850	600	52%
52	6.1	64%	450C	3547	2000	58%
53	5.8	55%	500C	2985	no	58%
54	4.6	43%	500C	2969	no	52%
59	3.2	34%	500C	3078	no	37%

a. Calculated by uranium mass collected on the cathode divided by uranium in the feed, nominally 9.5 kg.

3. DISCUSSION

3.1. Effect of Pulsating Current

In electrical plating practice it has been known for a relatively long time that the application of a periodical changing current, such as pulsating current, leads to improvements in the quality of the deposits obtained. Pulsating current consists of a periodic repetition of square or sinusoidal pulses. That is, the system is suddenly submitted to a current during a time interval and then left to relax for a period. As a matter of fact, the existence of the electrical shorting between anode baskets and vessel hardware has resulted in a pulsating current effect on the cathode during a direct transport in Mark-IV ER.

Table II. Summary of Three Cathodes Produced by Direct Transports under Different Shorting Conditions

Cathode No.	Average Vcell	Anode rpm	Cathode rpm	U Mass on Cathode, kg	Uranium Recovered By DT Process[a]	ER Temperature	Total A-h	~Shorting A-h	Current Efficiency
49	0.42	5	5	9.1	95%	450C	4628	4500	66%
52	0.39	5	5	6.1	64%	450C	3547	2000	58%
59	0.42	5	5	3.2	34%	500C	3078	No	37%

a. Calculated by uranium mass collected on the cathode divided by uranium in the feed, nominally 9.5 kg.

As anode baskets rotate in the ER salt phase, a momentary electrical shorting path is created between baskets and vessel when the FDBs touch the deposits on the metal ring beneath them. At the moment when the anode baskets touch the metal deposit, a spike current shows in the current curve and a sharp decrease occurs in the anodic voltage curve (a shorting path is "*on*"). Then the shorting path will be burned off by the high current passing through it or turned off by the rotating FDBs. After the removal of the shorting path the voltage and current values will return to normal (the shorting path is "*off*"). As the next shorting path builds up due to uranium dissolving from the anode baskets, another sharp decrease in voltage curve occurs, and so on. The fluctuations in the anodic voltage signals shown in Figure 7 support the described momentary electrical "*on*" and "*off*" phenomenon.

Figure 10 illustrates a conceptual model of the current distributions during a direct transport under the "shorting" conditions in Mark-IV ER. When the shorting path is *"off,"* the schematic current distribution is given in Figure 10(a), which is similar to the model shown in Figure 4. The uranium is being transferred from FDBs and the cadmium pool onto the cathode. The current distributes along the cathode/solution interface. When the shorting path is *"on,"* as is shown in Figure 10(b), the FDBs, cadmium pool, and vessel become a combined anode. The current distribution pattern under such conditions is somewhat similar to a deposition process. The majority of the uranium is being transferred from the cadmium pool onto the cathode. The current distribution is focussed mainly on the lower surface of the cathode.

As the shorting path *"on"* and *"off"* cycle continues, the current distribution pattern along the cathode/salt interface keeps changing alternately between Figures 10(a) and 10(b). It is this alternate "*on*" and "*off*" of the shorting path that generate a "pulsating current" effect on the cathode surface.

It is known that metal deposit formations by current or voltage pulses result in different nucleation and crystal growth conditions compared to a direct current deposition (10,11). A major effect of pulsating current electrochemical deposition is improvement in mass transfer process at the cathode/solution interface. When the anode FDBs periodically touch the ER vessel, a periodic relaxation of the diffusion field takes place at the cathode/salt interface. Since the ER is operated by controlled current mode, the relaxation of the diffusion field prevents the development of high concentration polarization at the cathode surface. This improves the crystal growth process at the cathode and leads formation of compact deposits.

3.2. Effect of Potential Gradient Along Cathode/Salt Interface

It has been reported that a stable cathode growth during an electrocrystallization process requires a high concentration of solute ions and a high effective electrical potential gradient at crystal-solution interface (12). The existence of electrical shorting between the anode baskets and ER vessel can alter cell voltage distribution, especially the voltage

gradient along the dendrite/molten salt interface, which favors a stable crystal growth on the cathode surface.

The electrical potential field calculations for a direct transport at snapshots of the shorting path "*on*" and "*off*" conditions have been performed by using FIDAP simulation code. The simulation details are reported in a separate paper (7). Figures 11 and 12 show the calculated potential contours when the shorting path is "*on*" or "*off*." It is assumed that the applied cell voltage is 0.4 V (from the minimum of -0.2 V to the maximum of 0.2 V). It can be noted in Figure 11 that when no shorting is taking place between the FDBs and ER vessel, the applied electrical potential field spreads from the anode (FDBs) to the vessel (cadmium pool) and from the vessel to the cathode. The calculated potential of the cadmium pool is ~ 0.11 V. When the shorting is taking place, FDBs, cadmium pool, and ER vessel are at the same potential, 0.2 V, and the applied electrical potential field distributes mainly within the quadrant in which the cathode mandrel is located (Figure 12). Apparently the potential gradient at crystal/solution interface is higher when anode baskets and ER vessel are shorted.

In order to quantitatively determine the difference in electrical potential and the potential gradient at the cathode surface when anode baskets and ER vessel are shorted or not shorted, modeling efforts were also made to calculate the electrical potential and potential gradient distributions at the cathode surface when a direct transport just commences. Figure 13 provides a comparison of the electrical potential distributions on a horizontal line through anode and cathode 30 cm above the bottom of the vessel when the anode baskets and the ER vessel are electrically shorted or not shorted. The calculated electrical potential gradients for the same horizontal line are also given in the figure. Figure 13 shows clearly that the electrical potential gradient at the cathode/solution interface is ~30% higher when anode baskets and ER vessel are electrically shorted. These simulated results are in good agreement with the experimental data presented in Tables I and II. The correlations between the calculate electrical potential gradients and experimental results also fit the morphology model proposed by Huggins and Elwell (12).

Furthermore, the "pulsating current" effect described in a previous section can change the current density and current density distributions alternately along the crystal-solution interface at the cathode. Since the electrorefining processes are operated by controlled current mode, the actual effect is the periodically changes in potential and potential gradient at cathode surface, which may also favor a stable crystal growth.

4. CONCLUSIONS

1. The cadmium pool acts as an intermediate electrode during direct transport process in the Mark-IV electrorefiner.

2. The cadmium level has gradually decreased due to its high vapor pressure and vaporization rate at the ER operational temperature.

3. The low cadmium level has caused the anode baskets momentarily touch the ER vessel hardware as the baskets are rotating, which generates a periodical electrical shorting path between the anode baskets and ER vessel during direct transport operations.

4. The existence of the periodical electrical shorting path makes the process of uranium dissolution from the anode baskets less effective, but appears to improve the morphology of cathode deposits.

5. The periodical electrical shorting between the anode baskets and the ER vessel has introduced a pulsating current effect to the system during the direct transports, and thereby improving the nucleation and electrocrystallization processes at the cathode.

6. The results of electrical potential field calculations using FIDAP code indicate that the presence of electrical shorting can increase the potential gradient at the salt/cathode interface by ~30%, which favors a stable crystal growth at the cathode.

4. ACKNOWLEDGMENTS

This work was sponsored by the U.S. Department of Energy, Office of Nuclear Energy, Science and Technology, under Contract W-31-109-Eng-38. The submitted manuscript was authored by a contractor of the U.S. Government. Accordingly, the U.S. Government retains a nonexclusive, royalty-free license to publish or reproduce the published form of this contribution, or allow others to do so, for U.S. Government purposes. Argonne National Laboratory is operated by the University of Chicago.

REFERENCES

1. Environmental Assessment: Electrochemical Treatment Research and Demonstration Project in the Fuel Conditioning Facility at Argonne National Laboratory-West, *DOE/ EA-1148*, U.S. Department of Energy, Department of Nuclear Energy, Science, and Technology (1996).

2. S. X. Li, R. D. Mariani, T. J. Battisti, and R. S. Herbst "Initial Results for the Electrochemical Dissolution of Spent EBR-II Fuel," Proceedings of the DOE Spent Nuclear Fuel and Fissile Materials Management, American Nuclear Society, Charleston, SC (September 8-11, 1998).

3. G. Boisde, G. Chauvin, H. Coriou et J. Hure, "Contribution a la Connaissance du Mecanisme de l'Electroraffinage de l'Uranium en Bains de sels Fondus," Electrochemica Acta, **5**, 54 (1961).

4. D. Inman, G. J. Hills, L. Young, and J. O'M Bockris, "Electrode Reaction in Molten Salt," Transactions of the Faraday Society, **55C**, 1904 (1959).

5. Smithells Metals Reference Book, 6th ed., E. A. Brandes, Editor, Butterworths (1983).

6. E. R. Van Artsdalen and I. S. Yaffe, J. Electrochem. Soc., **59**, 118 (1955).

7. T. Sofu, S. X. Li and R. A. Wigeland, "Electrical Potential Field Calculations for the FCF Mark-IV Electrorefiner," Proceedings of The 193rd Electrochemical Society Meeting, Xi-Eleventh International Symposium on Molten Salts, San Diego, CA (May 3-8, 1998).

8. T. Kobayashi et al., "Evaluation of Cadmium Pool Potential in a Electrorefiner with Ceramic Partition for Spent Metallic Fuel," J. of Nucl. Science and Technology, **34**, 50 (January 1997).

9. K. M. Goff, A. Schneider, and J. E. Battles, Nuclear Technology, **102**, 331 (June 1993).

10. A. R. Despic and K. I. Popov, "The Effect of Pulsating Potential on the Morphology of Metal Deposits Obtained by Mass-transport Controlled Electrodeposition," J. of Applied Electrochemistry, **1**, 275 (1971).

11. E. Budeski, G. Staikov, W. J. Lorentz, "Electrochemical Phase Formation and Growth,", VCH, 263 (1996).

12. R. A. Huggins and D. Elwell, "Morphological Stability of A Plane Interface during Electrocrystallization from Molten Salts," J. of Crystal Growth, **37**, 159 (1977).

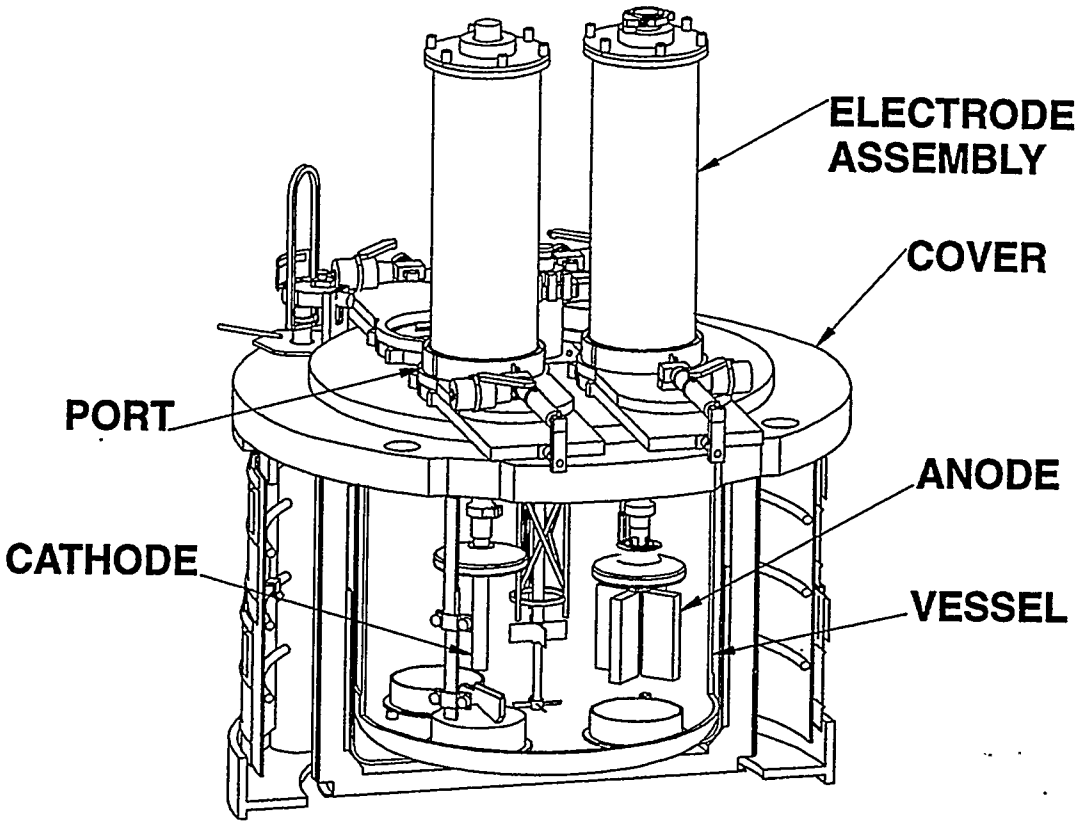

Figure 1. Schematic of Mark-IV Electrorefiner

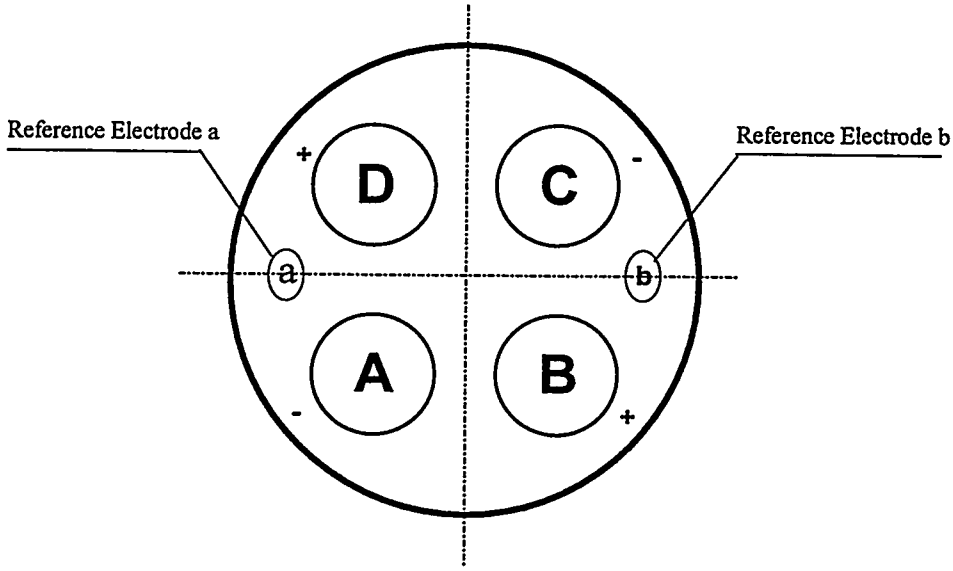

Figure 2. Port Configurations at Mark-IV Electrorefiner

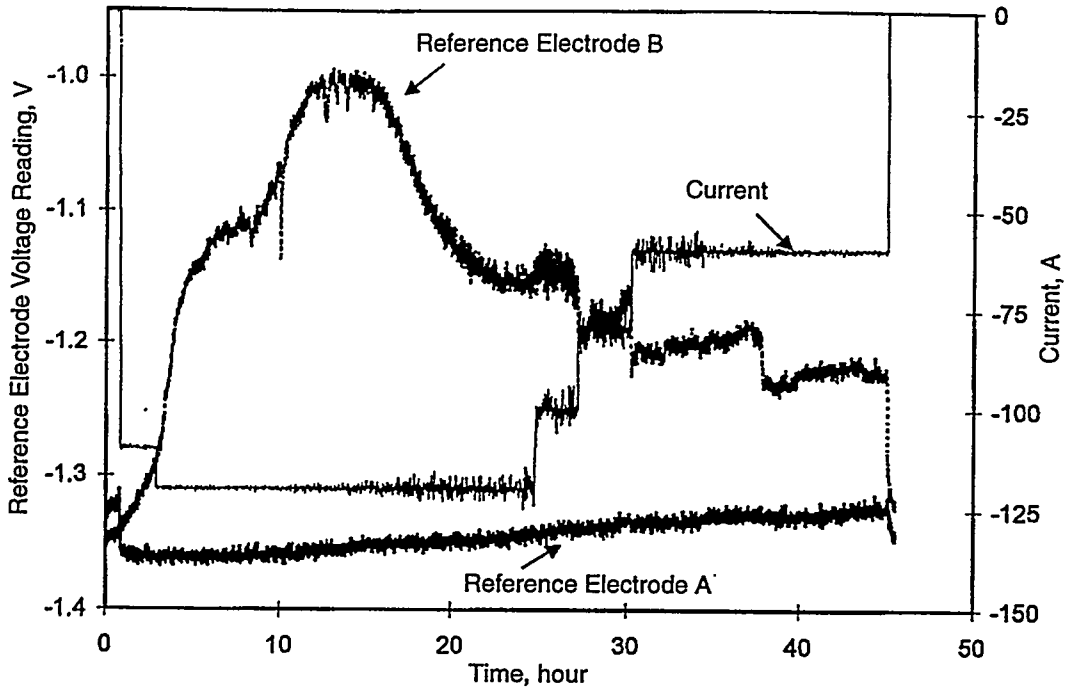

Figure 3. Reference Electrode Voltage Readings and Current during No. 29 Direct Transport in Mark-IV Electrorefiner

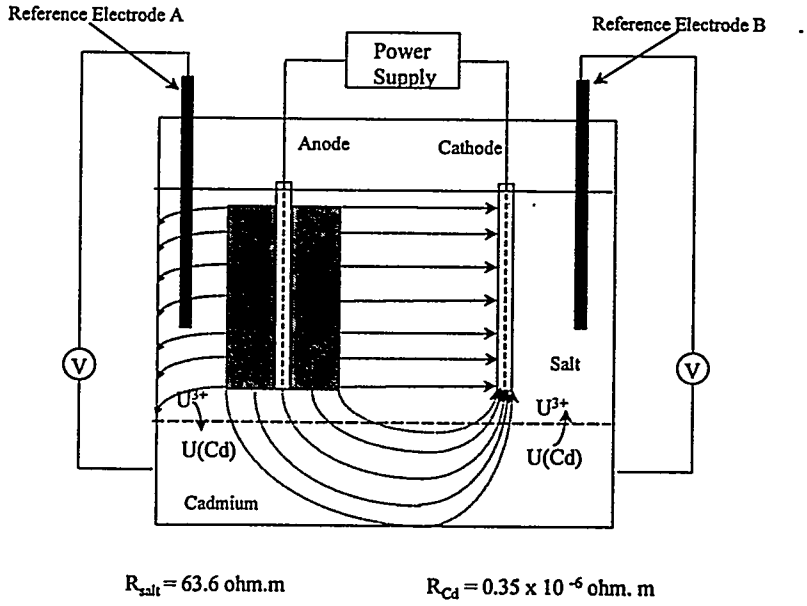

Figure 4. Schematic of Current Distribution Model during Direct Transport in Mark-IV ER

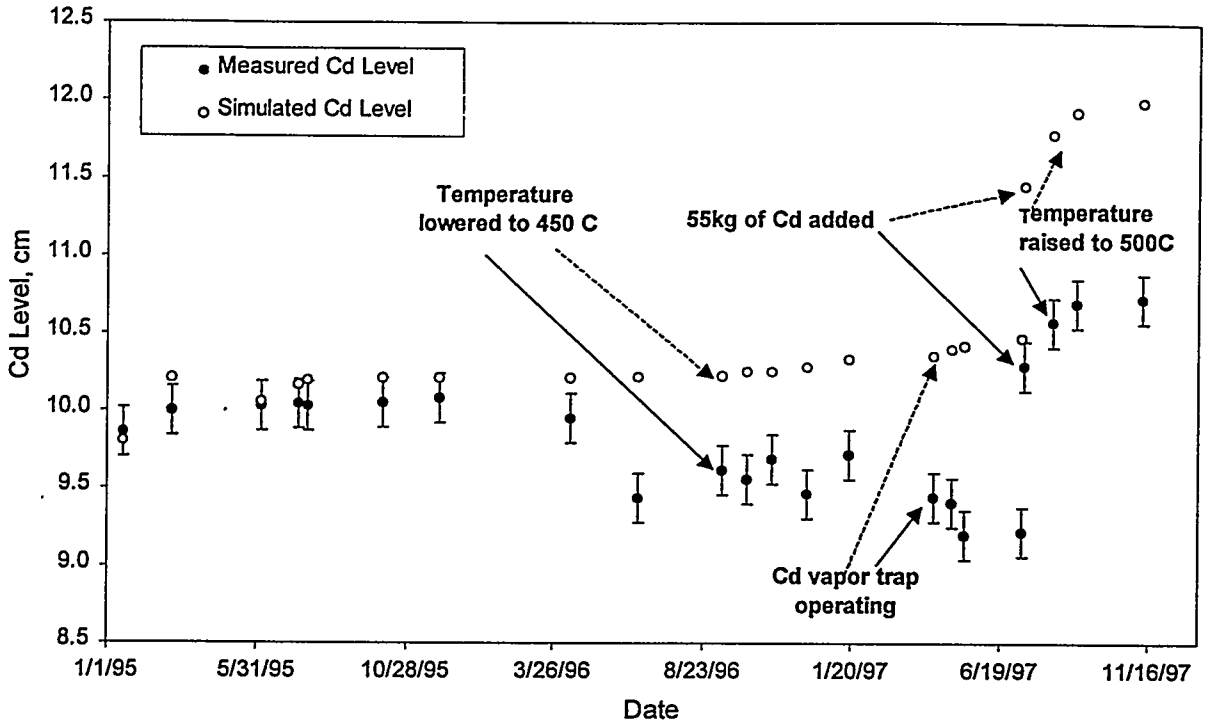

Figure 5. Measured and Simulated Cadmium Levels in Mark-IV Electrorefiner

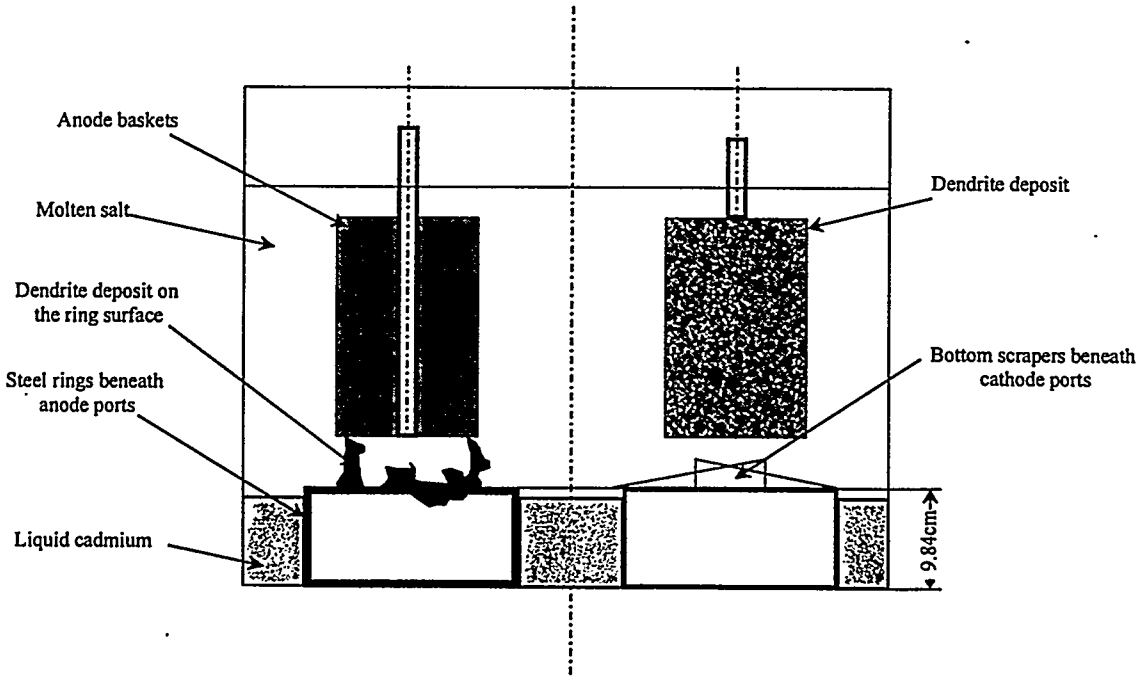

Figure 6. Schematic of Electrical Shorting between Anode Baskets and ER Vessel

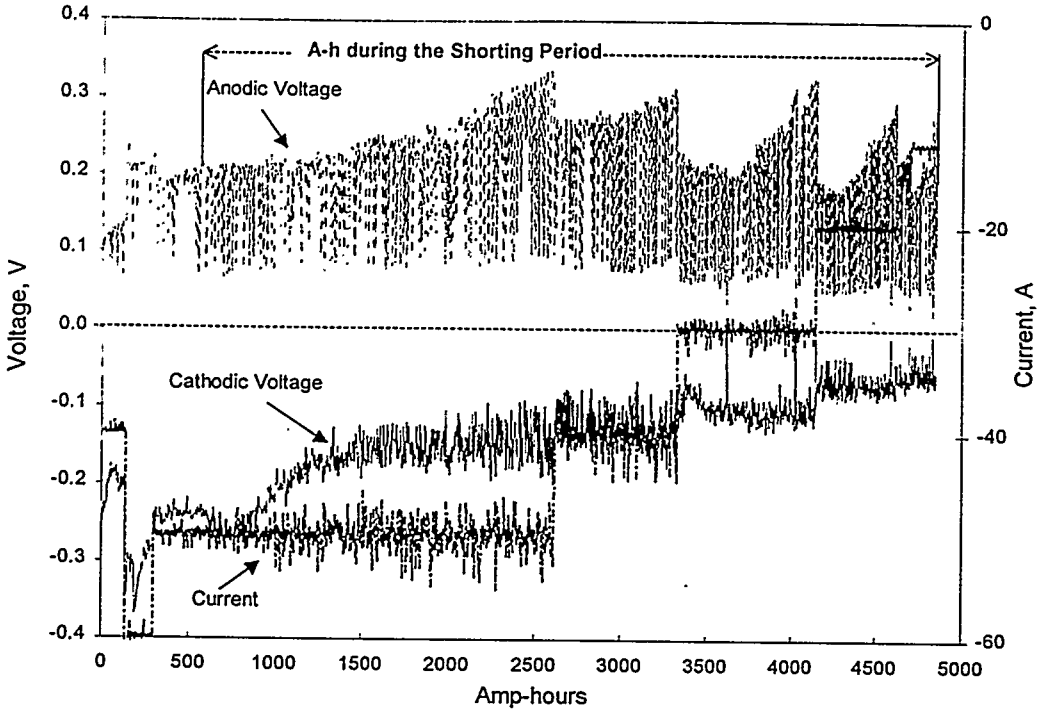

Figure 7. Typical Voltage and Current Traces during a Direct Transport when Anode Baskets are Electrically Shorted with the ER Vessel

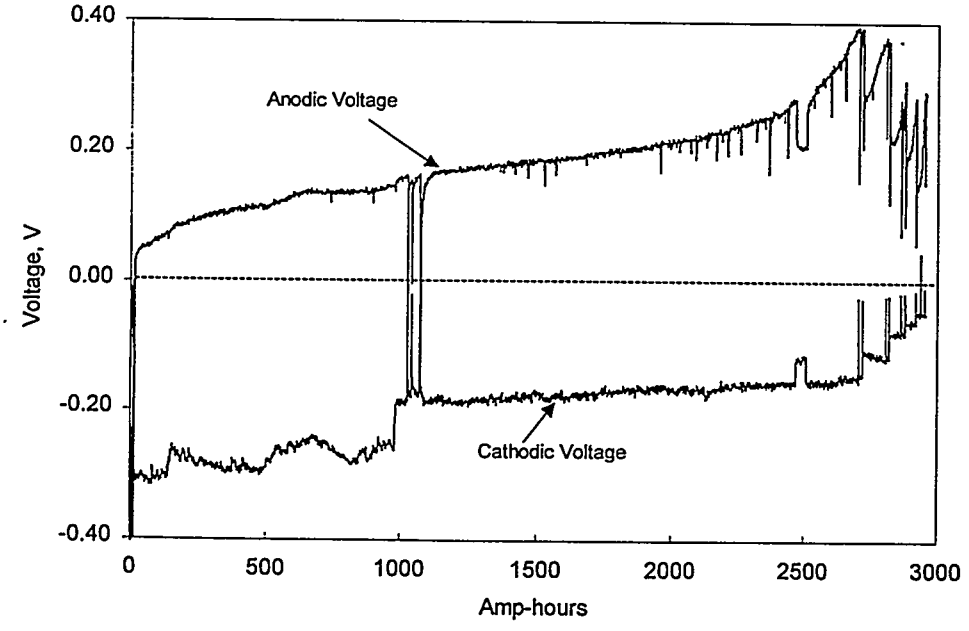

Figure 8. Typical Voltage and Current Traces during a Direct Transport when Anode Baskets are not Electrically Shorted with the ER Vessel

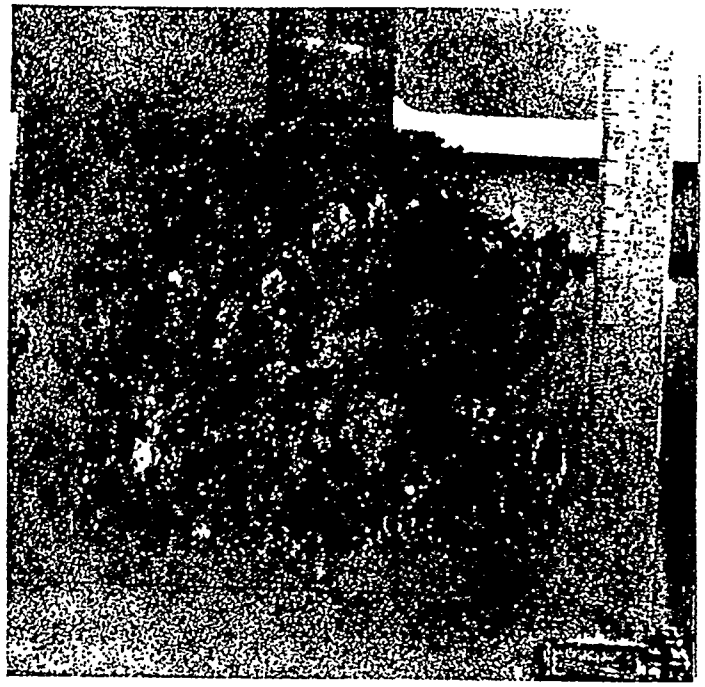

(A)
Figure 9. Cathode No. 49, 9.1 kg Uranium

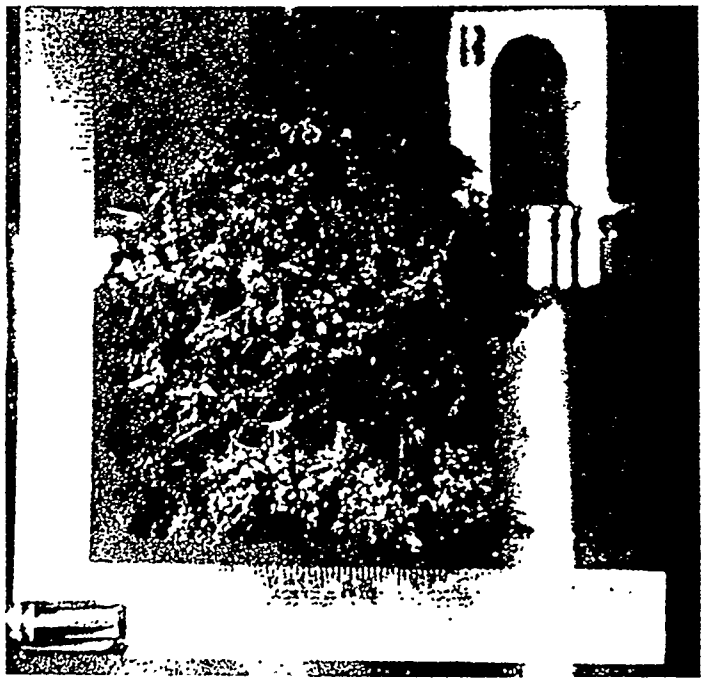

(B)
Figure 9. Cathode No. 52, 6.1 kg Uranium

(C)

Figure 9. (contd.) Cathode No. 59, 3.1 kg Uranium

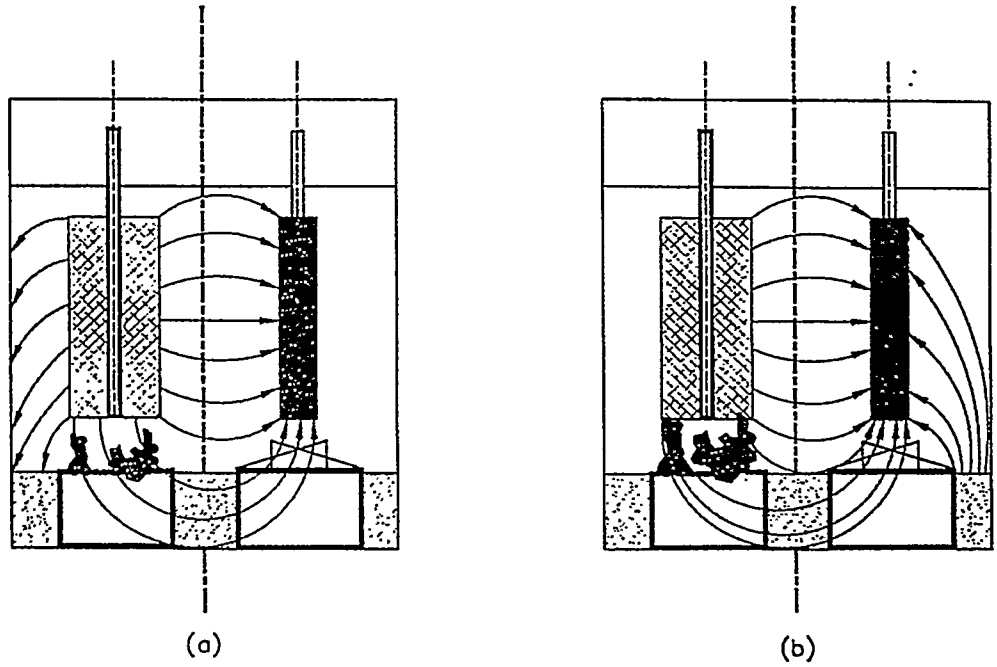

Figure 10. a. Current Distribution during a Direct Transport when "Shorting" is *"Off"*
b. Current Distribution during a Direct Transport when "Shorting" is *"On"*

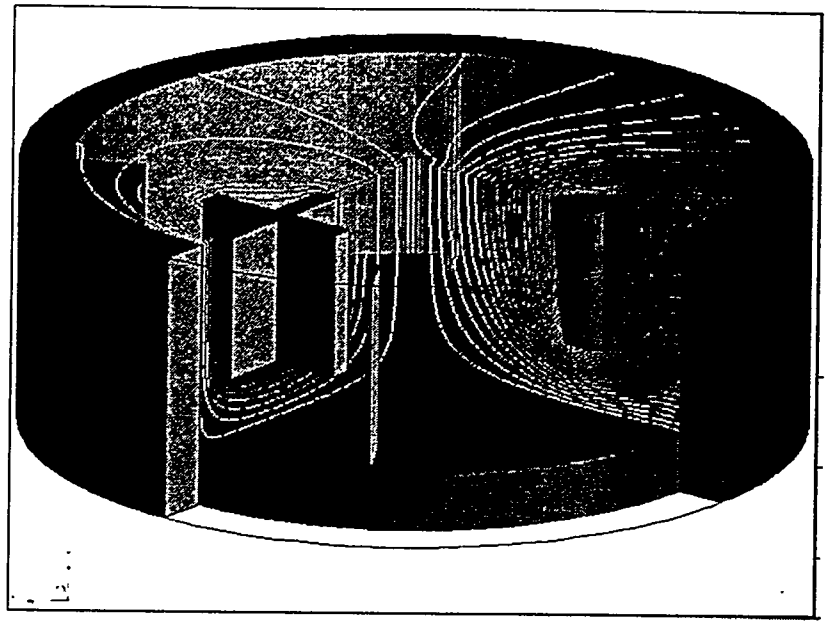

Figure 11. Electrical Potential Contours for a Direct Transport when Anode Basket are not Shorted with Vessel
(Constant Cell Voltage, 0.4 V)

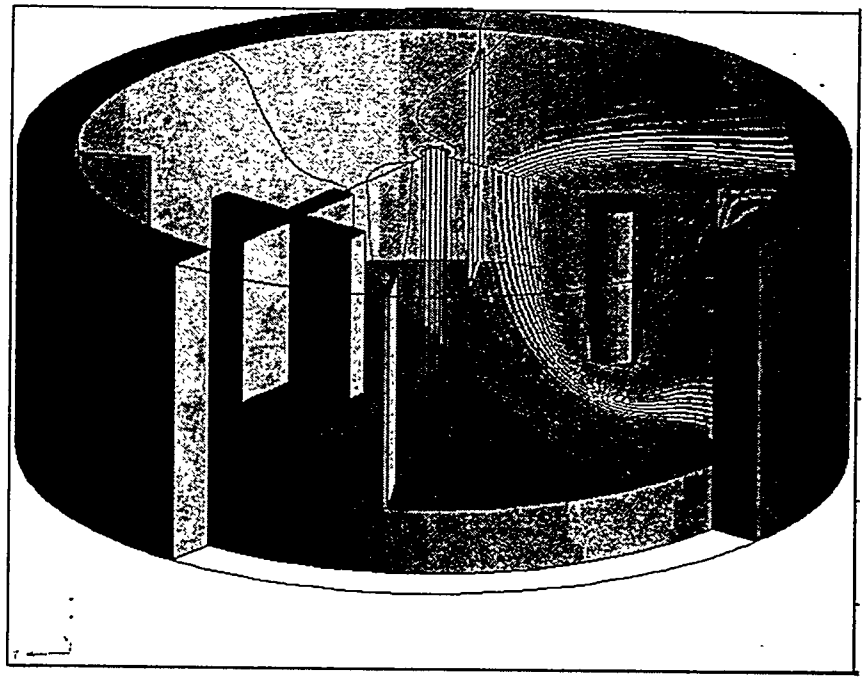

Figure 12. Electrical Potential Contours for a Direct Transport when Anode Basket are Shorted with VesselConstant Cell Voltage 0.4 V
(Constant Cell Voltage, 0.4 V)